International Journal of Nanomedicine

Dovepress
open access to scientific and medical research

Open Access Full Text Article

ORIGINAL RESEARCH

Mitigation of SARS-CoV-2 by Using Transition Metal Nanozeolites and Quaternary Ammonium Compounds as Antiviral Agents in Suspensions and Soft Fabric Materials

Israel Guerrero-Arguero[1], Siddiqur Rahman Khan[1], Brandon M Henry[1], Andreu Garcia-Vilanova[1], Kevin Chiem[1], Chengjin Ye[1], Sweta Shrestha[2], Deborah Knight[3], Mark Cristner[4], Shauna Hill[4], W James Waldman[3], Prabir K Dutta[2,5], Jordi B Torrelles[1], Luis Martinez-Sobrido[1], Amber M Nagy[1,4]

[1]Disease Intervention & Prevention and Population Health Programs, Texas Biomedical Research Institute, San Antonio, TX, USA; [2]ZeoVation Inc., Columbus, OH, USA; [3]Department of Pathology, The Ohio State University, Columbus, OH, USA; [4]Chief Scientist's Office of Science and Technology, 59th Medical Wing, Joint Base San Antonio-Lackland, San Antonio, TX, USA; [5]Department of Chemistry, The Ohio State University, Columbus, OH, USA

Correspondence: Prabir K Dutta; Amber M Nagy, Email dutta.1@osu.edu; AMallory@txbiomed.org

International Journal of Nanomedicine downloaded from https://www.dovepress.com/
For personal use only.

Introduction: The coronavirus disease 2019 (COVID-19) pandemic has demonstrated the need for novel, affordable, and efficient reagents to help reduce viral transmission, especially in high-risk environments including medical treatment facilities, close quarters, and austere settings. We examined transition-metal nanozeolite suspensions and quaternary ammonium compounds as an antiviral surface coating for various textile materials.

Methods: Zeolites are crystalline porous aluminosilicate materials, with the ability of ion-exchanging different cations. Nanozeolites (30 nm) were synthesized and then ion-exchanged with silver, zinc and copper ions. Benzalkonium nitrate (BZN) was examined as the quaternary ammonium ion (quat). Suspensions of these materials were tested for antiviral activity towards SARS-CoV-2 using plaque assay and immunostaining. Suspensions of the nanozeolite and quat were deposited on polyester and cotton fabrics and the ability of these textiles towards neutralizing SARS-CoV-2 was examined.

Results: We hypothesized that transition metal ion containing zeolites, particularly silver and zinc (AM30) and silver and copper (AV30), would be effective in reducing the infectivity of severe acute respiratory syndrome coronavirus 2 (SARS-CoV-2). Additionally, AM30 and AV30 antiviral potency was tested when combined with a quaternary ammonium carrier, BZN. Our results indicate that exposure of SARS-CoV-2 to AM30 and/or AV30 suspensions reduced viral loads with time and exhibited dose-dependence. Antiviral activities of the combination of zeolite and BZN compositions were significantly enhanced. When used in textiles, AM30 and AV30-coated cotton and polyester fabrics alone or in combination with BZN exhibited significant antiviral properties, which were maintained even after various stress tests, including washes, SARS-CoV-2-repeated exposures, or treatments with soil-like materials.

Conclusion: This study shows the efficacy of transition metal nanozeolite formulations as novel antiviral agents and establishes that nanozeolite with silver and zinc ions (AM30) and nanozeolite with silver and copper ions (AV30) when combined with benzalkonium nitrate (BZN) quickly and continuously inactivate SARS-CoV-2 in suspension and on fabric materials.

Keywords: SARS-CoV-2, disinfection, quats, zeolites, transition metals, coated fabrics

Plain Language Summary

The still ongoing COVID-19 pandemic unveiled the critical role of infection mitigation against emerging and re-emerging infectious diseases. Disinfection of contaminated surfaces is an effective transmission mitigation strategy, especially against highly transmissible pathogens and in high-risk settings, like hospitals, schools, or military living-quarters. Here, we tested a novel disinfectant technology that provided quick and continuous disinfection effect against SARS-CoV-2, the causative agent of COVID-19. This technology consists of two parts: benzalkonium nitrate, a quick acting ammonium-based disinfectant; and a zeolite nanostructure containing metal

Received: 14 January 2023
Accepted: 5 April 2023
Published: 3 May 2023

© 2023 Guerrero-Arguero et al. This work is published and licensed by Dove Medical Press Limited. The full terms of this license are available at https://www.dovepress.com/terms.php and incorporate the Creative Commons Attribution – Non Commercial (unported, v3.0) License (http://creativecommons.org/licenses/by-nc/3.0/). By accessing the work you hereby accept the Terms. Non-commercial uses of the work are permitted without any further permission from Dove Medical Press Limited, provided the work is properly attributed. For permission for commercial use of this work, please see paragraphs 4.2 and 5 of our Terms (https://www.dovepress.com/terms.php).

ions that provides the continuous disinfection effect. This technology can be used as coating in soft fabric materials (polyester and cotton) and maintains its disinfection effect. We also performed several stress tests and determined that the zeolite coating can resist repeated exposures to SARS-CoV-2, wash cycles, and covering in soil-like particles. In summary, we present a disinfection technology that not only provides instant but also a continuous effect against SARS-CoV-2 which can be used as a coating for clothes, surgical equipment, facemasks, tables and potentially many other porous or non-porous surfaces.

Introduction

Severe acute respiratory syndrome coronavirus 2 (SARS-CoV-2) is the causative agent of the coronavirus disease 2019 (COVID-19) pandemic, currently driving 12.3% and 0.123% of the world's infected population infected and deaths, respectively.[1] SARS-CoV-2 is an enveloped, single-stranded RNA virus, which mainly infects by the shedding of respiratory droplets secreted by infected humans. As these respiratory droplets are secreted, they are deposited on inanimate objects as fomites.[2,3] The relative risk of fomite transmission of SARS-CoV-2 is lower compared to direct contact with infected airborne droplets. However, there are reports of acquired SARS-CoV-2 infections being attributed to fomite transmission.[4,5]

The still ongoing COVID-19 pandemic has demonstrated the necessity for novel, affordable, and efficient agents to help reduce viral transmission, especially in high-risk exposure environments including medical treatment facilities, close quarters, and austere settings. The Environmental Protection Agency (EPA) has recently acknowledged the usefulness of reagents, whose activity can persist for extended periods.[6] Several nanostructured systems interspersed in personal protective equipment such as protective gear, masks, gloves, sheets, filtration units and paints have been studied to mitigate the infectious SARS-CoV-2 virus. Examples include ZnO, Mn, Fe, CuO, CeO_2, graphene oxide, TiO_2, Ni, Ag and Au in textiles, and have been recently reviewed.[7] Nanostructures including organic, polymeric, liposomes, micelles, lipid nanoparticles are also relevant for vaccine development and treatment methods.[8]

Amongst inorganic disinfectants, silver has been shown to have antimicrobial activity towards a broad spectrum of pathogens, and is also frequently used in medical treatments, including wound dressings and coatings, eg, on catheters.[9]

Metallic silver, in the form of silver nanoparticles (AgNP) also acts as broad antipathogenic agent against various bacteria, fungi, and viruses, including SARS-CoV-2,[9–11] and anticancer activity.[12] Optimization of AgNP to maintain high antimicrobial efficacy, along with minimizing toxicity is of significant research interest.[13,14] Besides studies of free suspended AgNP, immobilization studies of AgNP into various matrices, including lithographically patterned zeolite membranes, have been reported.[15] The AgNP-zeolite membrane was explored as an antimicrobial against *Escherichia coli* and its bactericidal properties were found to be mainly due to the gradual release of Ag^+ into the solution.[16] Other matrices in which AgNP have been incorporated are ceramics, plastics, metals, and various fabrics for applications as varied as catheters and wound dressings.[17–20] Studies with AgNP suggest that the mode of action is mediated by the release of silver ions, which have shown antiviral activity against human immunodeficiency virus-1 (HIV-1) through interaction with the gp120 surface glycoprotein, subsequently disrupting viral binding to CD4 receptors on host cells.[21] Additionally, several studies have identified AgNP antiviral activity against other viruses including double-stranded DNA disruption in HSV-1, interference of virus penetration into host cell in respiratory syncytial virus (RSV) and human parainfluenza virus (HPIV-3), virus-host cell binding blocking in HPIV-3 and monkeypox virus (MPXV), and inhibition of viral replication in influenza A virus (IAV).[22] Similar to silver, copper ions have also been shown to successfully inactivate bacteriophages,[23] thwart the infectivity of bronchitis virus,[24] and inhibit poliovirus RNA.[25] Together, copper and ferric ions have also been shown to inactivate herpes simplex virus (HSV), Junin virus (JUNV), and HIV-1.[23]

The above examples demonstrate the potential application of transition metals and ions as antipathogenic agents, including the use in high-density social environments like hospitals, schools, and office settings. However, free metal ions are susceptible to interaction with the environment and precipitation and inactivation, especially in the case of silver ions. This is one of the reasons that AgNP have gained research importance since they serve as a stable source of silver ions. However, AgNP typically have a surface coating in order to stabilize their nanoparticle size, and their dissolution is necessary for activity.[26] Zeolites are microscopic aluminosilicate porous materials.[27] Because of the framework negative charge of the zeolites, metal ions can be readily ion-exchanged into its pores/cages. This allows the use of silver directly in its ionic form, protected and stored in the cages of a zeolite, and has been studied.[28] Zeolites also allow the use of

multiple transition metal ions, all resident in the cages, which would be difficult to do with AgNP. Of particular interest to the SARS-CoV-2 and future pandemics is the use of materials loaded with Ag^+ ions, since these ions have already demonstrated antiviral effects against various viruses.[21,22,29,30] Most common real-world disinfectants are organic agents such as alcohol and quaternary ammonium compounds (quats). The advantage of the organics is that they destroy pathogens very quickly, in the order of minutes or less.[31,32] However, organic disinfectants require repeated reapplications and have health and environmental impact.[33]

The objective of this study was to examine the antiviral activity using a particular morphology of the faujasitic type of zeolite, namely with crystal sizes centered around ~30 nm.[34] Because of the colloidal nature of these zeolites, they afford long-term stability in suspension and can be used to coat various materials. Here we centered our efforts on studying metal containing zeolites as an efficacious coating on textiles and investigated their antiviral activity against SARS-CoV -2. The zeolites used in this study were ion-exchanged with Ag^+/Zn^{2+} (AM30) and Ag^+/Cu^{2+} (AV30). The antiviral capacity of AM30 and AV30 in suspension and as coatings on cotton and polyester fabrics against SARS-CoV-2 was elucidated. Additionally, we explored the resilience of the AM30/AV30 coatings when challenged with multiple adverse conditions, and the combined effect of AM30 and AV30 zeolite formulations with a quaternary ammonium compound (referred to as quat), benzalkonium nitrate (BZN). This study tested two hypotheses: first, that metal containing zeolite formulations are stable and can remain active as an antiviral agent for periods of time; and second that combination of transition metals and quats can provide an added synergistic antiviral effect. The latter would imply that lowered amounts of both reagents would be required, decreasing their health and environmental impact.

Materials and Methods

Zeolite Materials Assembly

Transition-metal ion-exchanged zeolite as 1% w/v suspensions in water were obtained from ZeoVation (Columbus, OH).[34] The three zeolite samples were Na^+-exchanged zeolite (ZC, served as zeolite control), Ag^+/Zn^{2+}-exchanged zeolite (AM30) and Ag^+/Cu^{2+}-exchanged zeolite (AV30). The transition metals were introduced by ion-exchange of ZC. BZN was prepared from benzalkonium chloride by exchanging the chloride anions with nitrate.

Zeolite Characterization

Particle size analysis of the AM30 and AV30 was performed by dynamic light scattering (DLS) and carried out on Malvern instrument (Zetasizer Nano ZS, Malvern Panalytical Inc., Westborough, MA). Diluted concentration of ZC (~0.1 wt.%) was prepared and sonicated for 10 min prior to measuring the DLS size. For powder X-ray diffraction (XRD) of ZC, AM30 and AV30 zeolites, the suspensions were centrifuged, the solids collected and dried in an oven at 100°C for 12 h, and ground to a fine powder. XRD patterns were obtained using Bruker X-ray diffractometer (Bruker D8 Advance Diffractometer, Bruker, Madison, WI) with Cu Kα radiation with 0.5 divergence, 0.02 step size, and 0.5 sec dwell time. The transition metal content of AM30 and AV30 was analyzed by Galbraith after acid dissolution using Inductively Coupled Plasma-Optical Emission Spectroscopy (ICP-OES, PerkinElmer, Waltham, MA).

Coating on Cotton Fabrics

Circular cotton fabric samples with 4.8 cm diameter were used for the coating. Coating was performed with 2 mL of 0.02 wt.%, 0.06 wt.%, 0.1 wt.% and 0.2 wt% BZN solutions loaded evenly on cotton fabrics targeting 22, 66, 110, and 220 μg/cm^2 of BZN, respectively. For the targeted loading of 100 μg/cm^2 of AM30 or AV30, 2 mL of 0.0905 wt.% of AM30 or AV30 suspensions were loaded evenly on the cotton fabric samples. The nanozeolite and quat coating on the textiles was done using the suspensions of the two materials. Using a dropper, the liquid was spread evenly across the textile running along the length of the textile. All cotton fabric samples were dried in an oven at 100°C for 10–15 min. In order to prepare AM30/BZN or AV30/BZN-coated cotton fabric samples, different concentrations of BZN (0.02 wt.%, 0.06 wt.%, 0.1 wt.%, 0.2 wt%) and AM30 or AV30 at 0.0905 wt.% were used to coat on cotton fabric samples sequentially. First, BZN was loaded on cotton fabrics and dried in the oven at 100°C for 10–15 min, followed by loading of AM30 or AV30 and drying in the oven at 100°C for an additional 10–15 min.

Coating on Polyester Fabrics

Circular polyester fabric samples with 4.8 cm diameter were used for the coating. Coating was performed with 0.4 mL BZN with 0.1 wt.%, 0.3 wt.%, 0.5 wt.% and 1 wt% loaded evenly on polyester samples targeting 22, 66, 110 and 220 μg/cm^2 of BZN, respectively. For the targeted loading of 100 μg/cm^2 of AM30 or AV30, 0.4 mL of 0.45 wt.% AM30 or AV30 suspensions were loaded evenly on the polyester fabric samples. The nanozeolite and quat coating on the textiles was done using the suspensions of the two materials. Using a dropper, the liquid was spread evenly across the textile running along the length of the textile. Note that the volume of suspension added to the polyester was lower than the cotton (though the absolute surface loading between both samples is the same by adjusting the suspension concentrations), due to the lower absorptivity of the polyester. All polyester fabric samples were dried in oven at 100°C for 5–10 min. In order to prepare AM30/BZN or AV30/BZN-coated polyester fabric samples, different concentrations of BZN (0.1 wt.%, 0.3 wt.%, 0.5 wt.%, 1 wt%) and AM30 or AV30 at 0.45 wt.% were used to coat on polyester fabric samples sequentially. First, BZN was loaded on polyester fabrics and dried in the oven at 100°C for 5–10 min, followed by loading of AM30 or AV30 and drying in the oven at 100°C for 5–10 min (different from the cotton since the polyester dried faster).

Cells and Virus

African green monkey kidney epithelial Vero E6 cells were obtained from the American Type Culture Collection (ATCC, Manassas, VA, USA; CRL-1586) and cultured in Dulbecco's Modified Eagle Medium (DMEM) (Thermo Fisher Scientific Inc, Waltham, MA, USA; Fisher Scientific MT15013CV) supplemented with 10% heat-inactivated Fetal Bovine Serum (FBS) (VWR International, Radnor, PA, USA; 97068–085) and 1% penicillin/streptomycin/L-glutamine (PSG) (Fisher Scientific 30–009-CI) solution. SARS-CoV-2, USA-WA1/2020 strain (Gen Bank: MN985325.1) was obtained from BEI Resources (NR-52281). SARS-CoV-2 USA-WA1/2020 was isolated from an oropharyngeal swab from a patient with a respiratory illness in January 2020 in Washington, USA. The virus stock obtained from BEI Resources was a passage 4 stock and was propagated to generate a master stock in Vero E6 cell cultures. Resulting stocks were titrated by plaque assay and quantified by immunostaining as described below.

Plaque Assay and Immunostaining

Confluent monolayers of Vero E6 cells (10^5 cells per well, 24-well plate format, triplicates) were infected with serial viral dilutions for 1 h at 37°C. After viral adsorption, the viral inoculum was removed and washed 2× with PBS. Cells were then overlaid with post-infection media containing DMEM/F12 Nutrient Mixture (Thermo Fisher Scientific Inc, Waltham, MA, USA; Gibco 12500–062) supplemented with 0.35% bovine serum albumin (Sigma-Aldrich, St. Louis, MO, USA; A74409), 1% PSG, 0.25% sodium bicarbonate (Thermo Fisher Scientific Inc, Waltham, MA, USA; Fisher Chemical S233), 1% Ultrapure Agarose (Thermo Fisher Scientific Inc, Waltham, MA, USA; Invitrogen 16500), 0.02 M HEPES (Corning Inc., Corning, NY, USA; 25–060-CI) and incubated at 37°C in a 5% CO_2 incubator. At 72 h post-infection (hpi), cells were fixed overnight with 10% neutral buffered formalin solution (Sigma-Aldrich, St. Louis, MO, USA; HT501128). For immunostaining, cells were permeabilized with 0.5% (v/v) Triton X-100 (Sigma-Aldrich, St. Louis, MO, USA; X100) in PBS (Thermo Fisher Scientific Inc, Waltham, MA, USA; Gibco 10–010-049) for 15 min at room temperature and immunostained using the SARS-CoV cross-reactive nucleocapsid (N) protein 1C7C7 monoclonal antibody (MAb, 1 μg/mL) (Leinco Technologies, Inc, St. Louis, MO, USA; LT7000) and the Vectastain ABC kit (Vector Laboratories, Inc., CA, USA; PK4002), followed by secondary antibody binding and developing using the DAB Peroxidase (HRP) Substrate kit (Vector Laboratories, Inc, CA, USA; SK4100). After immunostaining, plates were scanned and photographed using a ChemiDoc MP Imaging System (Bio-Rad Laboratories, Inc, Hercules, CA, USA; 17001402).

Suspension Zeolite Testing Against SARS-CoV-2

Zeolite suspensions were prepared by 1 min sonication in a water bath sonicator (Branson 1510; 1510-MT) and 10-fold serially diluted in PBS. SARS-CoV-2 suspension (250 μL at 10^5 PFU/mL) was mixed with the previously prepared zeolite suspensions at a 1:1 (v/v) and incubated at room temperature with constant oscillation (200 RPMI) for the corresponding contact time. Zeolites were inactivated by adding 0.05% (m/v) TG (Spectrum Chemical, New Brunswick, NJ, USA; SO209) and incubated for 10 min. The neutralized samples were serially diluted in DMEM 2% FBS 1% PSG and plated in 24-well plates containing Vero E6 cells for plaque assay titration and quantification by immunostaining as previously described.

Zeolite-Coated Fabrics Testing

To recover SARS-CoV-2 from tested fabrics, fabrics were cut in 1×1 inch-squares and placed in 12-well plates. SARS-CoV-2 suspension (200 µL at 10^6 PFU/mL) was directly deposited on fabrics and incubated at room temperature at pre-determined contact times (10 minutes contact time (mCT), 2 hour contact time (HCT) CT, 24 HCT). To inactivate the zeolites, 300 µL 0.05% (m/v) TG was added and incubated for 10 min at room temperature. The neutralized sample was transferred to a 15 mL conical tube containing 4.5 mL of DMEM 2% FBS 1% PSG and vortexed for 1 min at maximum speed. The supernatant was transferred to a clean tube and serially diluted for plaque assay viral titration and quantification by immunostaining.

Washing Protocol for Polyester Samples

For deionized (DI)-water washes, in a 100-mL jar, 15 stainless steel balls and 30 mL of DI water were added. For detergent washes, 2 mL of detergent (Tide Liquid Detergent, Procter & Gamble, Cincinnati, OH) was added to 28 mL DI-water. Coated fabric samples (4.8 cm diameter) were placed in the jar. The jar was sealed properly and placed in a Burrell Scientific Wrist Action Model 75 Laboratory wrist shaker holder (Burrell Scientific 0757750419, Zelienople, PA). Five washing cycles were carried out continuously at a setting of 10 speed (~250 rpm) for a total of 225 min. Fabric-coated samples were rinsed with DI-water if washed with detergent. Then, the coated fabrics were dried in an oven at 100°C for 5 to 15 min. Control samples were not washed.

Soil-Like Particles Coating Treatment of Samples

Soil load mix was prepared by mixing 0.5 g of bovine serum albumin (BSA, Sigma-Aldrich, St. Louis, MO) in 10 mL PBS, 0.5 g yeast extract (Sigma-Aldrich, St. Louis, MO) in 10 mL PBS, and 0.04 g of mucin (Bovine Submaxillary Gland, EMD Millipore Corp., Burlington, MA) in 10 mL PBS. For SL100 samples, 100 µL of soil load mix was evenly loaded on the top of BZN, AV30 or AV30/BZN-coated polyester samples (4.8 cm diameter) and control samples and allowed to dry at RT. For SL200 samples, 200 µL of soil load mix was evenly loaded on those coated polyester samples and control samples and allowed to dry at room temperature.

Evaluation of Combinatory Effect of Zeolite and BZN Formulations

Combined zeolites and BZN formulations were diluted from 10,000 ppm to 0.01 ppm (10-fold dilutions) and from 50 ppm to 0.75 ppm (2-fold dilutions), respectively. The resulting solutions were inoculated with approximately 200 PFU of SARS-CoV-2 and incubated at room temperature for 10 mCT. To inactivate the zeolites within the solution, 50 µL of 0.05% (m/v) TG was added and incubated for 10 min at room temperature. The neutralized sample was transferred to a 96-well plate with previously seeded Vero E6 cells (10^4 cells/well seeded overnight). After 1 h of adsorption, the inoculum was removed and overlay media was added DMEM supplemented with 2% FBS, 1% PSG, 1% Avicel (Sigma-Aldrich, St. Louis, MO, USA; 11365) and incubated at 37°C in a 5% CO_2 incubator. After 24 h incubation, plates were fixed with 10% neutral buffered formalin and plaques were quantified by immunostaining as previously described. This assay was performed three times in triplicate.

Cell Viability Assay

Diluted concentrations of AM30/AV30 (10-fold) and BZN (2-fold) were mixed in a checkerboard pattern on a 96-well plate. Resulting solutions were inactivated for 10 min at room temperature with TG (0.05%) before being transferred to 96-well plates with confluent monolayer of Vero E6 cells (10^4 cells/well seeded overnight) and incubated for 10 min at 37°C in a 5% CO_2 incubator. The Cell proliferation kit II (XTT) (Roche Holding AG, Basel, CH; Cat. No. 11465015001) labeling mixture was prepared according to manufacturer's instructions, 50 µL per well of the mixture was added and incubated for 4 h at 37°C. After incubation, plates were read in a plate reader for absorbance at 570 nm with a reference wavelength of 650 nm. This assay was performed three times in triplicate.

Statistical Analysis

Statistical significance was determined by using either a two-way ANOVA with Dunnett's multiple comparisons test or Holm–Sidak's multiple *t*-tests against untreated controls. All data are presented as mean ± SEM for each group and

analyzed using Prism v9.0 software (GraphPad Software, San Diego, CA). A P value <0.05 was considered statistically significant. P-values are denoted as *<0.05, **<0.01, ***<0.001, and ****<0.0001.

Results

Zeolite and BZN Characteristics

The porous zeolite structure examined in this study belongs to the faujasite family of zeolites and shown in Figure 1A. This zeolite has an internal surface area of ~600m^2/g and can be accessed through the 0.74-nm windows with entry into the 1.3-nm supercage.[27] A high-resolution transmission electron micrograph (HRTEM) of the as-synthesized Na^+-containing zeolite particles is shown in Figure 1B. The particles are uniformly shaped, with the average size being ~30 nm, and generate clear dispersions when suspended in water.[34] Dynamic light scattering (DLS) data of the suspensions of as-synthesized zeolites are shown in Supplemental Figure 1A, with an average particle size of approximately 70 nm. It is commonly observed that DLS predicts slightly larger size than electron microscopy.[35] Synthesized Na^+ zeolites (zeolite control, ZC) were ion-exchanged with Ag^+/Zn^{2+} in the AM30 sample (Ag wt %- 4.35%, Zn wt%- 0.56%) and Ag^+/Cu^{2+} in the AV30 sample (Ag wt%- 4.01%, Cu wt%- 0.45%, elemental analysis was done by ICP-OES). These transition metal ions occupy positions in the supercages and can be released in the presence of ionic media. Supplemental Figure 1B and C show the powder X-ray diffraction of the AM30 and AV30 zeolites, where all the peaks can be assigned to the faujasite structure of Figure 1A.[34] The structure of benzalkonium nitrate (BZN), a monoquaternary ammonium compound, is shown in Figure 1C. In the presence of zeolite, the positively charged BZN can associate with the negative surface charge of the zeolite as shown in Figure 1D.

Zeolites and BZN Disinfectant Activity in Suspension

We initially tested zeolite formulations and BZN in suspension at various concentrations and different contact times against SARS-CoV-2 (~10^4 PFU/mL). These included AV30 and AM30 at 10,000, 1000, 100, 10, 1, 0.1, 0.01 parts per million (ppm) for 2, 4 and 24 HCT (Figure 2A–C), and BZN at 500, 250, 100, 40, 20, 10, 5 ppm for 10 mCT (Figure 2D). Na^+-zeolite (ZC) served as controls for all the zeolite experiments. Sodium thioglycolate (TG) was used to

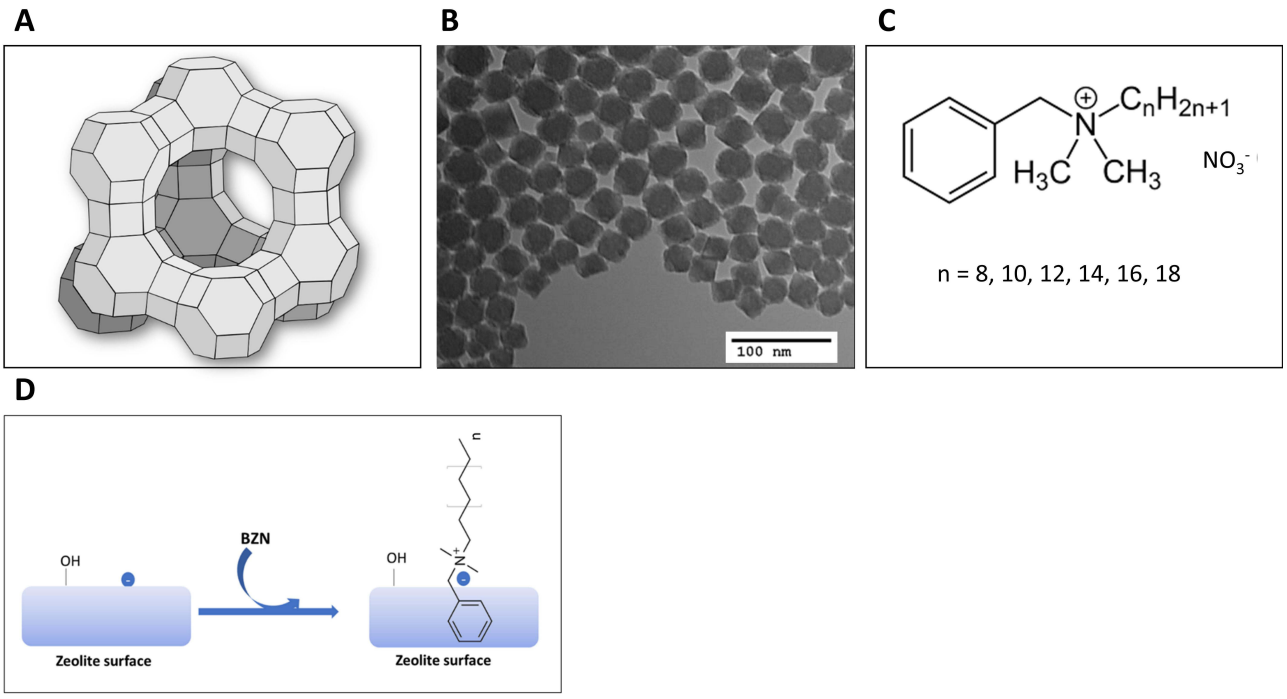

Figure 1 (**A**) Schematic of a zeolite supercage of the faujasite family of zeolites (**B**) High-resolution transmission electron microscope (TEM) images of nanozeolite particles. Scale bar = 100 nm. (**C**) Structure of the quat benzalkonium nitrate (BZN). (**D**) Binding of positively charged BZN to a negatively charged zeolite surface.

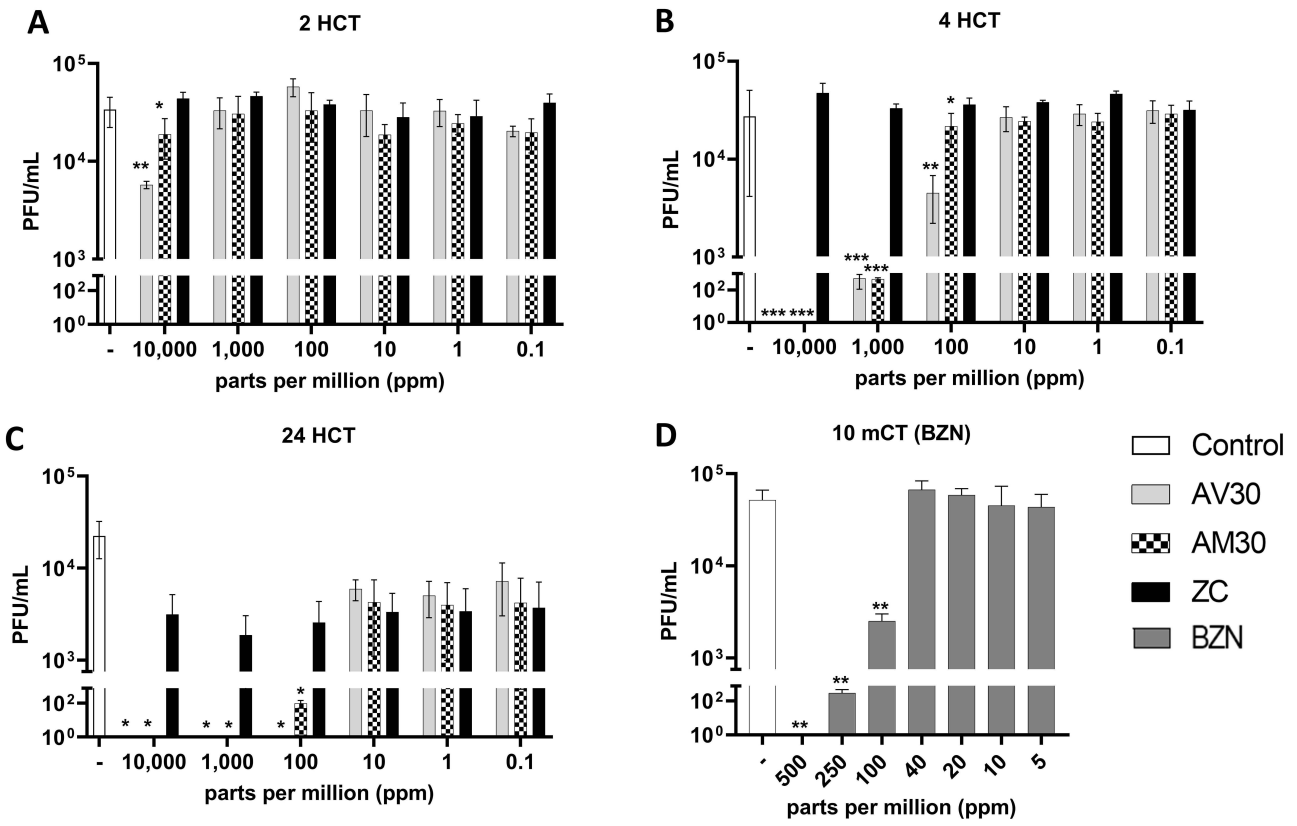

Figure 2 (**A**) 2 HCT (hour count, 2h), (**B**) 4 HCT (hour count, 4h) and (**C**) 24 HCT (hour count, 24h) exposure of AM30, AV30 and zeolite control (ZC) in suspensions at concentrations of 0.1, 1, 10, 100, 1000 and 10,000 ppm to SARS-CoV-2 (**D**) 10 mCT (minute count, 10 min) challenge of SARS-CoV-2 against 5, 10, 20, 40, 100, 250 and 500 ppm BZN in suspension. Error bars show SEM, N=3. Statistical significance was determined using Holm–Sidak's Multiple comparisons *t*-test. *P<0.05, **P<0.01, ***P<0.001.

neutralize transition metal ions prior to the virus assay with Vero E6 cells. We demonstrated that the presence of TG did not have a significant impact on the Vero E6 cell viability by using the XTT cell proliferation assay (the reduction of XTT by cellular oxidoreductase enzymes produces a water-soluble formazan which is detected via an absorbance-based microplate reader) (Supplemental Figure 2).

We observed moderate to significant reduction of viral load of AV30 and AM30 formulations at 10,000 ppm concentration within 2 HCT (Figure 2A). At this concentration, the efficacy of AV30 and AM30 increased over time starting with 1-$\log_{10}$ and 0.5-$\log_{10}$ at 2 HCT, respectively. After 4 HCT (Figure 2B), no viable virus was recovered at 10,000 ppm. At lower concentrations (100 to 1000 ppm), AV30 and AM30 impact on virus titers was effective at 4 HCT with approximately 2-$\log_{10}$ reduction for 1000-ppm concentration, and with ~1 $\log_{10}$ and 0.25 $\log_{10}$ reduction at 100-ppm concentration for AV30 and AM30, respectively. At lower concentrations, AV30 and AM30 maintained effectiveness in reducing virus titers at 24 HCT (Figure 2C). Indeed, all suspensions of 10,000, 1000, and 100 ppm of both AV30 and AM30 showed full inhibition potency (~3.5-$\log_{10}$) at 24 HCT, except for AM30 at 100 ppm with a ~1.5-$\log_{10}$ reduction compared to the inoculum viability. We observed a slight reduction of the viral inoculum viability at 24 HCT in our zeolite control (ZC) vs the control with no particle treatment, adding ~1-$\log_{10}$ reduction in viral titers related solely to the presence of Na^+-zeolites (Figure 2C). There was destabilization of the virus if treated with the zeolite control for 24 h. To assess the activity of soluble BZN, we tested its inactivation potency against SARS-CoV-2 at 10 mCT. We observed a dose-dependent effect of BZN against SARS-CoV-2, with the highest BZN concentration of 500 ppm resulting in undetectable viral titers (~4.5-$\log_{10}$ reduction), and 250 ppm and 100 ppm driving a ~2.5 $\log_{10}$ and ~1 $\log_{10}$ reduction, respectively (Figure 2D).

Anti-SARS-CoV-2 Effectiveness of Combinations of Zeolite and BZN-Coated Cotton and Polyester Fabrics

We next determined the most effective combinations of zeolite/BZN formulations in coated polyester and cotton fabric samples using fixed concentrations of AM30 and AV30 (at 100 μg/cm^2) and different concentrations of BZN (at 22, 66, 110 and 220 μg/cm^2). The units of concentration used in this paper are weight of actives per unit area of the textile surface, which allows for comparing antiviral efficacy of different samples directly. Some authors do use concentrations of actives per weight of the support. For that reason, we provide the average weight of cotton fabric (4.8 cm diameter) to be 1.2505 ± 0.0836 g and weight of polyester fabric (4.8 cm diameter) to be 0.3734 ± 0.0069 g. Coated, dried textiles appeared unchanged upon visible inspection, and these were tested several weeks after the coating.

We evaluated the viral reduction potency of these formulations after a short contact time with SARS-CoV-2 (10 mCT), as well as evaluated their continuous effect on the virus at 2 and 24 HCT.

In cotton fabrics, at 10 mCT, and 2 and 24 HCT, our results show that formulations containing BZN alone (220 μg/cm^2) or in combination with AM30 or AV30 (100 μg/cm^2) had undetectable SARS-CoV-2 upon viral deposition on the coated fabrics (~5 $\log_{10}$ reduction) (Figure 3A–C). However, at 10 mCT, AM30 alone did not have significant effect, and AV30 alone exhibited 0.5 $\log_{10}$ reduction. The effects of AM30 and AV30 alone were more obvious over time both at 2 and 24 HCT, with a ~2 $\log_{10}$ reduction at 24 HCT (Figure 3C).

We also observed a dose-dependent effect linked to the applied concentration of BZN with the cotton fabrics. At 10 mCT, BZN alone did not completely inhibit SARS-CoV-2 growth when used at 22 and 66 μg/cm^2 for coating materials, but the concentration of 110 μg/cm^2 was effective (Figure 4). However, when BZN was combined with AM30 or AV30, SARS-CoV-2 inhibition was observed at lower BZN coating concentrations, with full inhibition at 66 μg/cm^2 and ~1.5 $\log_{10}$ inhibition at 22 μg/cm^2 (Figure 4).

In polyester fabrics, we observed a similar pattern of SARS-CoV-2 inhibition upon deposition at 10 mCT and 24 HCT (Figure 5A and B) as noted for cotton fabrics (Figure 3A and C) with BZN (220 μg/cm^2) and AM30 or AV30 (100 μg/cm^2). AV30 alone was more effective than AM30 at both challenge times.

We also carried out dose-dependency testing with polyester samples (Figure 6). Samples containing 22 μg/cm^2 concentration of BZN resulted in ~1-$\log_{10}$ reduction alone; a more pronounced decrease was observed when BZN was combined with AM30 or AV30 (100 μg/cm^2) (Figure 6). Compared to cotton fabric (Figure 4), BZN coating at 66 μg/cm^2 fully inhibited SARS-CoV-2 growth in polyester fabric (Figure 6).

Effects of Combinations of Zeolites and BZN

From the data shown above, there are clear hints that AV30 appears to be more effective in combination with BZN over AM30. To get a better grasp of the behavior between the two zeolite samples, we set up an assay where it was possible to investigate a range of concentrations of the zeolite and BZN in a single experiment. Figure 7A shows the experimental design, much like

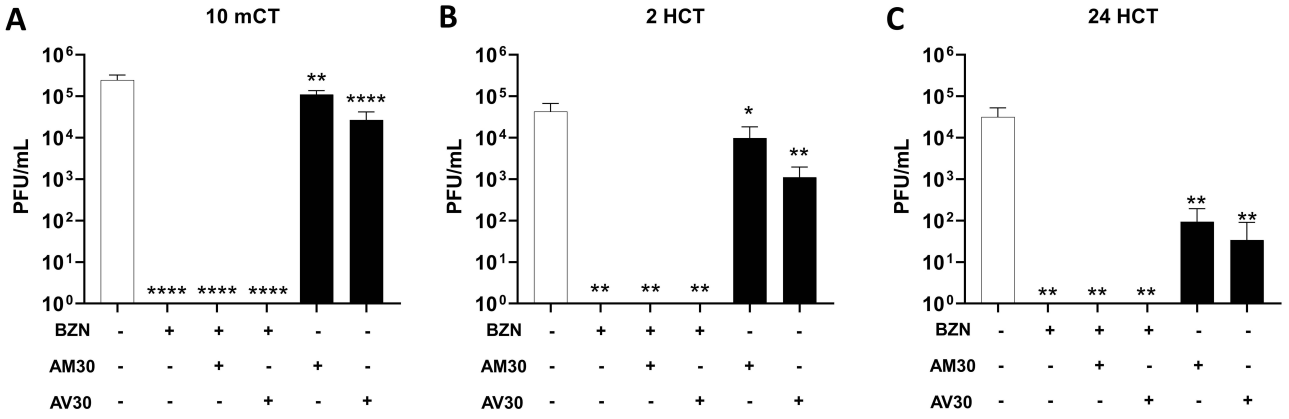

Figure 3 Zeolite-coated cotton fabrics exposed to SARS-CoV-2 for (**A**) 10 mCT (minute count, 10 min) and (**B**) 2 HCT (hour count, 2h) and (**C**) 24 HCT (hour count, 24h). Concentrations of actives used were BZN (220 μg/cm^2), AM30 and AV30 (100 μg/cm^2). + Sign indicates the presence of the actives and – sign indicates its absence. Error bars show SEM, N=3. Statistical significance was determined using 2-way ANOVA multiple comparisons. *P<0.05, **P<0.01, ****P<0.0001.

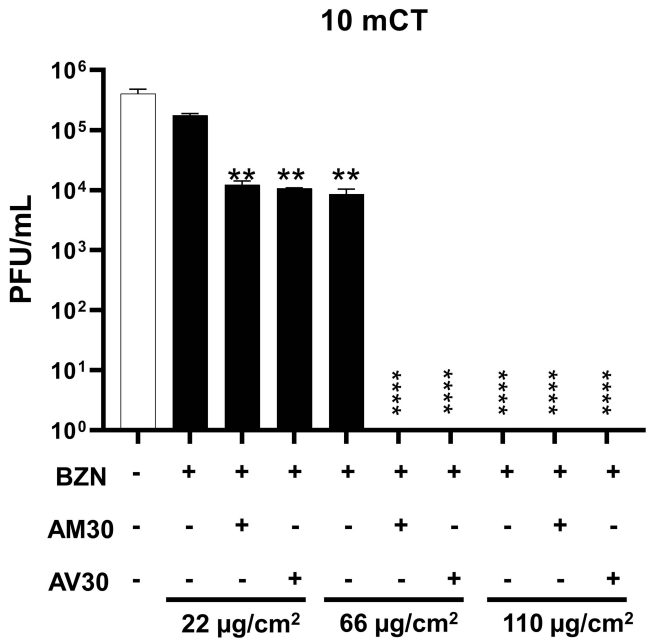

Figure 4 Zeolite-coated cotton fabrics with variable concentrations of actives exposed to SARS-CoV-2 for 10 min (10 mCT- ten-minute count). Concentrations of actives used were: BZN (22, 66, and 110 µg/cm^2); AV30 and AM30 (100 µg/cm^2). + Sign indicates the presence of the actives and – sign indicates its absence. Error bars show SEM, N=3. Statistical significance was determined using 2-way ANOVA multiple comparisons. **P<0.01, ****P<0.0001.

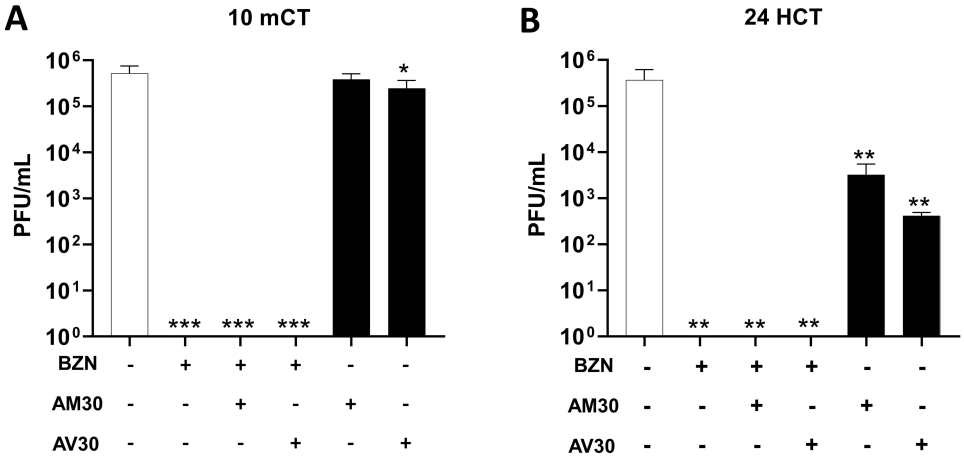

Figure 5 Zeolite-coated polyester fabrics exposed to SARS-CoV-2 for (**A**) 10-mCT (minute count, 10 min) and (**B**) 24 HCT (hour count, 24 h). Concentrations of actives used were: BZN (220 µg/cm^2), AM30 and AV30 (100 µg/cm^2). + Sign indicates the presence of the actives and – sign indicates its absence. Error bars show SEM, N=3. Statistical significance was determined using 2-way ANOVA multiple comparisons. *P<0.05, **P<0.01, ***P<0.001.

a checkerboard assay in which the concentration of zeolite was varied from 0.001 to 10,000 ppm (in units of 10), and the BZN from 0.42 to 50 ppm (in units of 2) in a multi-well plate. The resulting zeolite and BZN solutions were inoculated with approximately 200 PFU of SARS-CoV-2 and incubated at room temperature for 10 mCT. Plaques were counted in each of the wells. Supplemental Figure 3A and B show a photograph of the plaques in each well of the plate after the completion of the 10 min experiment and Supplemental Figure 4A and B show the plot of PFU reduction for all concentrations studied (normalized to the controls). Of particular interest was determination of the lowest concentrations of the combination of zeolite and BZN that resulted in 100% plaque reduction (no plaques observed). These data are plotted in Figure 7B. For AM30, 100 ppm of zeolite did reduce plaque count to zero in the presence of 50 ppm BZN. For AV30, 10 ppm of zeolite along with 6.75 ppm of BZN, as well as 1 ppm of zeolite with 50 ppm of BZN reduced plaque count to zero (note that the concentration of SARS-CoV -2 in these experiments were 200 PFU/mL, as compared to suspensions and textiles of 10^{5-6} PFU/mL). In combination with

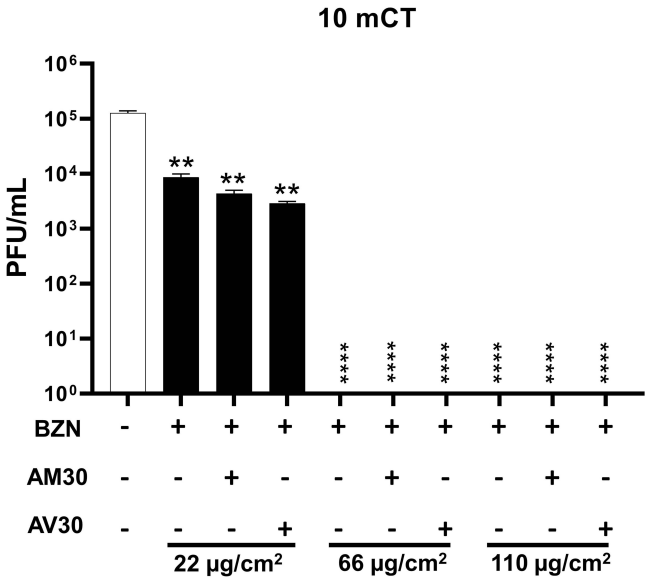

Figure 6 Zeolite-coated polyester fabrics with variable concentrations of actives exposed to SARS-CoV-2 for 10 min (10 mCT- ten-minute count). Concentrations of actives used were: BZN (22, 66, and 110 µg/cm^2); AV30 and AM30 (100 µg/cm^2). + Sign indicates the presence of the actives and – sign indicates its absence. Error bars show SEM, N=3. Statistical significance was determined using 2-way ANOVA multiple comparisons. **P<0.01, ****P<0.0001.

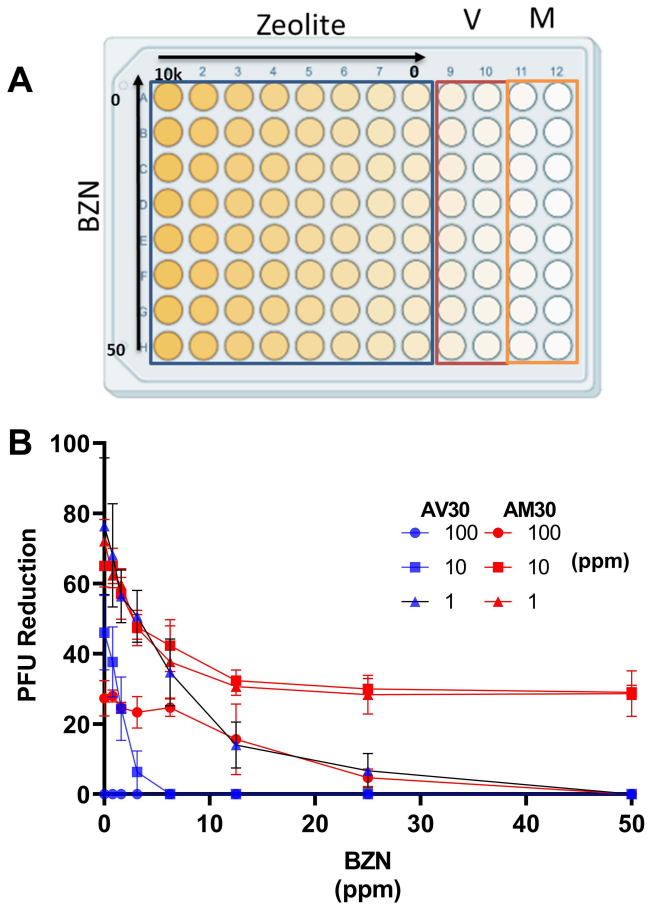

Figure 7 (**A**) Arrangement of the 96-well checkerboard pattern for testing variable concentrations combining BZN (0–50 ppm in steps of 2) and AM30 or AV30 (0–10,000 ppm in steps of 10). V and M columns indicate virus-only and mock controls, respectively. (**B**) Two-variable concentration checkerboard-pattern assay of AV30 and AM30 at 100, 10, and 1 ppm with 0–50 ppm BZN.

BZN, AV30 clearly outperforms the AM30 as antiviral agent. This has implications for the amount of quat and zeolite used in practical applications; additionally, incorporation of lower reagent quantities has less potential on environmental impacts.

Resiliency of Zeolite-Coated Fabrics Against Soil-Like Particles, Wash Cycle Simulations, and Repeated Viral Insults

To determine the virus inactivation lifespan of the coated zeolite textiles, additional characterization of the fabrics was conducted by exploring their resilience against simulated wash cycles, with and without detergent, and soil-like materials (meant to simulate organic dirt in real-world use). These experiments were only conducted with AV30, because this compound demonstrated higher potency than AM30, and all samples were analyzed after 10 minutes of contact time with virus. SARS-CoV-2 titer reduction was examined on polyester fabrics coated with BZN (66 μg/cm^2), or combinations of BZN (66 μg/cm^2) with AV30 (100 μg/cm^2). Antiviral activity remained potent after fabrics were washed for 5 cycles with only distilled water (~5-log$_{10}$ reduction) and virus was subjected to subsequent 10-minute exposures. However, samples washed with detergent through 5 cycles had its antiviral activity significantly compromised providing only ~1-log$_{10}$ reduction in viral viability for both BZN (66 μg/cm^2) or combinations of BZN (66 μg/cm^2) with AV30 (100 μg/cm^2) (Figure 8A).

To explore further the resilience of the tested formulations deposited on polyester fabrics, an additional coating of soil-like particles was applied to coated fabrics. The simulated soils were prepared as recommended by EPA and included bovine serum albumin, yeast extract and mucin (SL100 and SL200 −100 and 200 μL of soil solution applied uniformly on 4.8 cm diameter textile).[36] Our results indicate that either treatment with BZN (66 μg/cm^2) or combinations of BZN (66 μg/cm^2) with AV30 (100 μg/cm^2) did not affect the antiviral activity against deposited SARS-CoV-2 on the soiled textile, with an observed ~5 log$_{10}$ reduction (Figure 8B).

Finally, we evaluated coating performance after challenge with multiple SARS-CoV-2 insults/depositions of the same highly concentrated viral inoculum (2 × 10^6 PFU/mL). This experiment was to simulate repeated exposures of virus during real-world use. Five different samples of the same polyester fabric, coated with BZN (66 μg/cm^2), or combinations of BZN (66 μg/cm^2) with AV30 (100 μg/cm^2), or uncoated (control) were exposed to SARS-CoV -2. After 10 minutes, one of the samples was analyzed and serial depositions of the same SARS-CoV-2 dose was

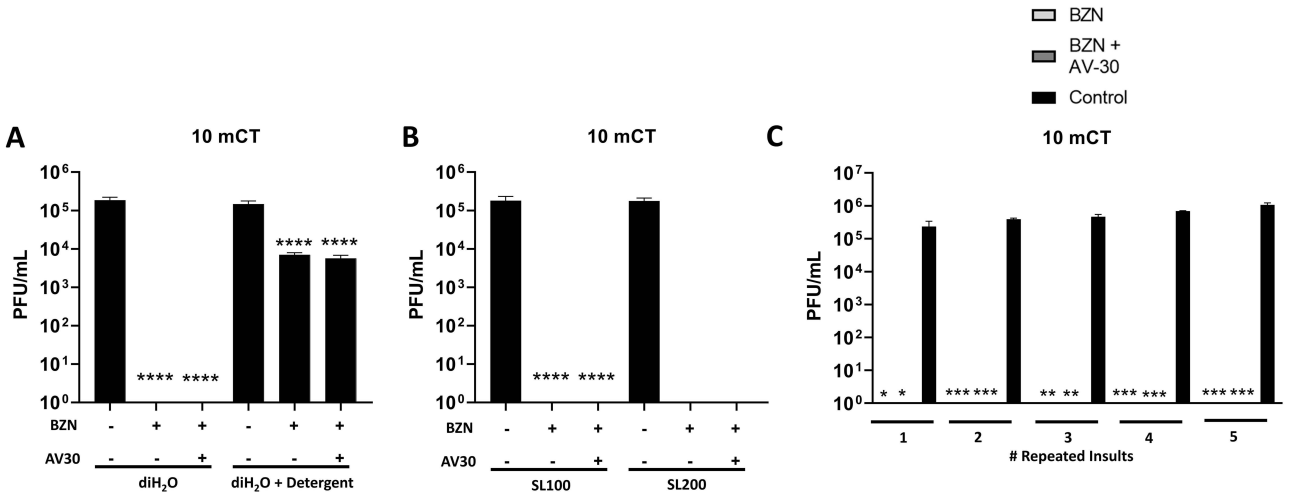

Figure 8 (**A**) Testing of the antiviral potency of coated polyester samples to washing with water and detergent. Exposure time to SARS-CoV-2 for 10 min (10 mCT) of BZN-coated with or without AV30 samples previously subjected to 5 cycles of simulated wash with or without detergent. Concentrations of actives used were: BZN (66 μg/cm^2) and AV30 (100 μg/cm^2). + Sign indicates the presence of the actives and – sign indicates its absence. (**B**) Testing of the antiviral potency of coated polyester samples exposed to soil loads (soil solution was made by mixing three solutions of 0.5 g of bovine serum albumin in 10 mL PBS, 0.5 g yeast extract in 10 mL PBS, and 0.04 g of mucin in 10 mL PBS). Exposure time of 10 min (10mCT) to SARS-CoV-2 of BZN-coated with or without AV30 polyester samples previously treated with soil-like particles, SL100 or SL200. Concentrations of actives used were: BZN (66 μg/cm^2) and AV30 (100 μg/cm^2); SL100 (soil load = 5.5 μL/cm^2), SL200 (soil load = 11 μL/cm^2). + Sign indicates the presence of the actives and – sign indicates its absence. (**C**) Testing of the antiviral potency of coated polyester samples after 5 repeated insults with SARS-CoV-2 each for 10 min (10 mCT) for BZN-coated with or without AV30. Concentrations of actives used were BZN (66 μg/cm^2) and AV30 (100 μg/cm^2). The experiment began with 5 textile samples on which the virus was deposited. After 10 min, one of the textile pieces was analyzed for virus, and the rest was treated with a similar viral load as the first sample. This process was repeated 5 times. Error bars show SEM, N=3. Statistical significance was determined using 2-way ANOVA Multiple comparisons. *P<0.05, **P<0.01, ***P<0.001, ****P<0.0001.

done on the remaining 4 samples. After 10 min, the second of the samples was analyzed and the viral dose repeated on the rest. This process was repeated for all five samples. We observed that both formulations, BZN and BZN + AV30, continued to exhibit ~5 $\log_{10}$ reduction after five consecutive challenges (Figure 8C).

Discussion

Minimizing infection of SARS-CoV-2 requires methods that can reduce the viral transmission by inactivating the virus. On surfaces accessible to touch, this can be done by coating the surface with suitable antivirals. Transition metal ions based on Cu^{2+} or Ag^{+} ions have been extensively explored as antimicrobial and antivirals, particularly within the antimicrobial field.[10,11,16,22,37,38] Of particular interest, the use of transition metals embedded in various matrices and in the form of metal nanoparticles as well as surface coatings have shown some promise in inactivating SARS-CoV -2.[11,39,40] In this study, we tested the effectiveness of two novel formulations (AM30/AV30) containing a combination of transition metal ions embedded in a nanozeolite matrix against SARS-CoV-2. The advantage of using nanozeolites is that stable suspensions are formed. This has two implications, in suspensions the zeolite with the transition metal ion cargo is always accessible to pathogens, because of lack of settling, and secondly, the suspension can be uniformly applied on surfaces, as we have done in this study on textile surfaces. We also characterized the antiviral activity of transition metal ion nanozeolites in combination with the quat BZN and further simulated the resilience of the formulation applied to textiles against various stress tests, including detergent washing and simulated soiled samples.

Inactivation of SARS-CoV-2 in suspension exhibited a strong time- and dose-dependent effect for the zeolite suspensions studied, with the Ag^{+}/Cu^{2+} containing AV30 formulation being the most potent formulation, leading to complete inhibition of viral activity at 24 h exposure at 100 ppm zeolite concentration (3.5 $\log_{10}$ decrease relative to control) (Figure 2). The Ag^{+}/Zn^{2+} containing formulation (AM30), albeit with lower potency, remains a viable option. We also observed a dose-dependent effect of BZN, a quaternary ammonium compound, with 500 ppm BZN completely suppressing viral activity at 10 min (4.5 $\log_{10}$ decrease relative to control). Both AM30 and AV30 act as long-term effect disinfectants, whereas BZN rapidly neutralizes the viral inoculum within 10 minutes.

Our initial observations on dose- and time-dependent, and BZN-driven enhancement of disinfectant potency in solutions were also maintained when these formulations were used in coated textile fabrics. There were some differences in the cotton and polyester samples examined. BZN alone at concentrations of 66 μg/cm^2 completely inhibited SARS-CoV-2 deposited in polyester-based fabrics (Figure 6); interestingly, this was not the case for cotton-based fabrics, as BZN at this same concentration only was efficient when combined with zeolites (Figure 4). This could be explained by the structural differences between polyester and cotton fabrics. Typically, cotton is more hydrophilic compared to polyester, the hydrophilic nature requiring stronger formulations as neutralizers.[41] Previous studies with cotton impregnated with quats have also shown loss of antiviral potency, due to the tight binding of the quat via the association of the positive charge of the quat with the hydroxylic groups in cellulose.[42,43] Assessment of these formulations' impact in the host cells' viability confirmed an artifact finding above 1000 ppm for both zeolite combinations, most likely due to the high scattering of the particles in the solution (Supplemental Figure 2).[44]

An important aspect of characterizing the viability of these formulations for real-world situations was to evaluate the textiles against three common stress-tests: repeated deposition/insult, endurance against washing both with and without detergent, and covered with soil-like materials. Although the AV30/BZN formulation was still effective after five wash cycles with distilled water, its potency was reduced significantly when detergent was added (Figure 8A). Because of their hydrophobic nature, detergents can remove the BZN, and could be the reason for the decrease in potency. Soil exposure testing did not reduce the antiviral potency of AV30/BZN coating against deposited SARS-CoV-2 viability (Figure 8B). Finally, we observed that AV30/BZN fabric-coating continued to complete kill of SARS-CoV-2 when virus inoculum was deposited five sequential times on the fabric (Figure 8C).

We conclude the discussion by focusing on the mechanistic aspects, related to two observations. First, the observed higher antiviral activity of AV30 over AM30, evident in the suspension as well as the textile samples. The suspension studies shown in Figure 2 consistently demonstrate that AV30 is more potent for AM30, eg, at 100 ppm zeolite for 24 h exposure, AV30 shows complete virus inactivation, and 3.5 $\log_{10}$ decrease, whereas AM30 shows a 1.5 $\log_{10}$ decrease. Note that the actual concentration of the active transition metals in the 100 ppm zeolite samples are in low ppm range.

For AV30, 4 ppm of Ag^+ and 450 ppb of Cu^{2+} is present, whereas for AM30, it is 4.35 ppm of Ag^+ and 560 ppb of Zn^{2+}. The zeolite is serving as a vehicle for delivery of the ions. Zeolite impregnated cotton and polyester samples (Figures 4 and 6) show the same trend, with AV30 exhibiting a ~1 $\log_{10}$ decrease advantage over AM30. Numerous studies on the three transition metals as antiviral, antimicrobial and antifungal agents have been reviewed recently.[45–47] The propensity of these metal ions to bind ligands containing P, N, O and S is the primary pathway of antipathogenic activity. The metal ions can interfere with virus binding to the host cell, interfere with the viral activity inside infected cells, and prevent the virions from being released from the host cell[48–50]. Silver can interact with viral envelope and viral surface proteins, as well as altering viral replication by interaction with the viral genome.[51] AgNP deactivates HIV-1 by damaging the envelope proteins, eg, glycoprotein gp120 on HIV-1, compromising the virus structure, and reducing infection by preventing binding to the receptor on host cells.[21,52] The virucidal effect of copper (both Cu^{2+} and Cu^+) is manifested by interaction with the viral genome, diminishing viral infectivity.[53] Copper can also form reactive oxygen species that can disrupt the viral envelope or capsid.[54] Zinc has been shown to inhibit proteolytic cleavage, disrupting synthesis of viral polypeptides, interfering with viral replication.[55] There are only few studies with combination of metals, in the form of metal alloys,[53] and do not serve as a good comparison with the present ion-based studies. The zeolite support provides a method to introduce these mixtures of transition metal ions co-localized spatially and temporally. It is difficult to conceive of another support that can protect the ions from the complex biological milieu and yet are available upon interaction with the pathogen. Based on the literature, though, it is unclear why the Ag^+/Cu^{2+} combination is more potent than Ag^+/Zn^{2+} as an antiviral towards SARS-CoV-2, and more studies are required.

The second observation is the enhanced effect when AM30 or AV30 is combined with BZN. Just focusing on the 10 min exposure result, the combined effect is most evident in the cotton sample. With BZN at 66 μg/cm^2, only 1 $\log_{10}$ decrease in viral activity is observed (Figure 4). AM30 alone at 100 μg/cm^2 show a 0.5 log decrease (Figure 3), whereas AV30 at 100 μg/cm^2 exhibit a 1-log decrease (Figure 3). However, if the BZN and AM30 or AV30 are combined on the cotton specimen, then a decrease of 4–5 $\log_{10}$ activity is observed, with complete loss of viral infectivity (Figure 4). Moreover, the experiment with varying concentrations of BZN and AM30 or AV30 in suspension in Figure 7 shows that AV30 and BZN form a more potent combination, eg, with 50 ppm BZN, it requires 100 ppm AM30, and 1 ppm AV30 for complete viral reduction (note that the viral titer here was smaller (200 PFU/mL) than the suspension and textile experiments (10^{5-6} PFU/mL). The higher potency of AV30 over AM30 when studied as individual regents transfers over to the mixtures with BZN.

Based on the literature, we provide a scenario as to why the quat zeolite combination is more potent. The virus is about 91±11 nm in size[56,57] and the zeolite particles are 30 nm in size, so it is unlikely that the nanozeolite particles will penetrate into the virus. Thus, the mechanism of activity of the zeolite can start only via introduction of the active transition metals onto the virus surface. Moreover, we observe a strong time-dependent increase in viral activity with the nanozeolites, with negligible effect at 10 min, and with significant effect at 24 h (Figure 2). Even concentrations as high as 10,000 ppm nanozeolite do not exhibit a quick effect (10 min). Quite the opposite effect is observed with the quat, leading to complete viral inactivation in 10 minutes at 500 ppm (Figure 2). It is well established that the mechanism behind quats as rapid disinfectants against envelope viruses is due to the disruption of the viral lipid envelope, as observed for HIV, hepatitis B virus and influenza virus.[49,58–61] Thus, the transition metal ions and the quat can act by different mechanisms, the quat being active on contact with the virus surface,[62,63] whereas the metal ions can penetrate through the viral surface coating, getting access to internal virus functionalities (which in all likelihood takes longer time). Support for the hypothesis that the viral envelope acts as a shield towards metal ions comes from the few studies that compare the antiviral activity of the same material towards envelope and non-envelope viruses. In a study with Ag^+/Cu^{2+} containing micron-sized zeolites towards envelope human coronavirus 229E and non-envelope feline calicivirus, it was found that with exposure to same amount of zeolite (10 wt% zeolite with 6.5 wt% Cu and 3.5 wt% silver impregnated on plastic plates), the viral activity towards the non-envelope virus was significantly higher than the envelope virus.[64] With 24-hour exposure, there was a 1.77 $\log_{10}$ decrease in 229E and 5.05 $\log_{10}$ decrease in the feline virus. Another example is AgNP deposited on graphene oxide (GO-Ag), whose antiviral activity was tested with envelope feline coronavirus (FCoV) and non-envelope infectious bursal disease virus (IBDV). With 1 mg/mL of GO-Ag, 22.7% of infection was inhibited in DF-1 cells with 9×10^5 $TCID_{50}$/mL of IBDV. With 1 mg/mL of GO-Ag, there was

no change in infection by 10^6 $TCID_{50}$/mL of FCoV to DF-1 cells as compared to a control GO without silver (8.4% inhibition of GO-Ag versus 7.2% infection inhibition by GO-Ag).[37] These studies suggest that the transition metals are more active towards non-envelope viruses.

Note that this situation is exactly the opposite of what is observed with quats and organics, which are more potent towards envelope viruses. For example, quats were effective in disrupting enveloped influenza A (H1N1), but not the non-envelope poliovirus Sabin.[65,66] With the envelope viruses, the transition metal ions need to penetrate through the envelope, whereas it can interact directly with the capsid of the non-envelope virus. With increasing concentration of the transition metal ions and time, the propensity of penetration through the envelope increases.

Since this study has not focused on the mechanistic aspects of the nanozeolite+quat antiviral activity, we cannot propose a detailed mechanism. However, based on the extensive literature on both silver and quats, we can hypothesize the quat zeolite combination works effectively because they work in a synergistic fashion. Here, we are defining synergy as one of the actives (quat) used is facilitating the activity of the second active (silver/copper). First, since the surface of the zeolite is negatively charged and quats carry a positive charge, there will be a strong Coulombic association between the zeolite and quat, as depicted in Figure 1D, implying that they will approach the virus as a unit. Studies of quat interactions with lipid membranes, especially as found in bacteria suggest a progression of structural changes with increasing concentration of the quat, and should be similar in the envelope virus.[67] These are depicted in Figure 9. Negative charges on the membrane surface attract the quat. At low concentrations, the quat long chain interdigitates into the lipid layer of the membrane driven by hydrophobic forces. With increasing amounts of quat, small hydrophilic pockets are built up, which gradually increases in size. At the highest concentration of quats, the hydrophobic lipids in the membrane get solubilized, and the membrane disintegrates, leading to virus death. We propose that at the low concentrations of quat, where small hydrophilic pockets are created, the positively charged transition metal ions from the zeolite can make their way into the membrane and then into the virus itself, interacting with the proteins and nucleic acids and inactivating the virus. The synergetic effect arises since small amounts of quat make it possible for the transition metal ions to access the interior of the virus, thus reducing the need for higher concentrations of the transition metals. In this scenario, with low concentration of both quat and the transition metal ion, the virus is deactivated. The quats tend to be more effective antimicrobial agents than antiviral agents, and so typically higher concentration of quats are required for antiviral activity.[60] This is because in antimicrobial activity, altered envelope permeability by binding of

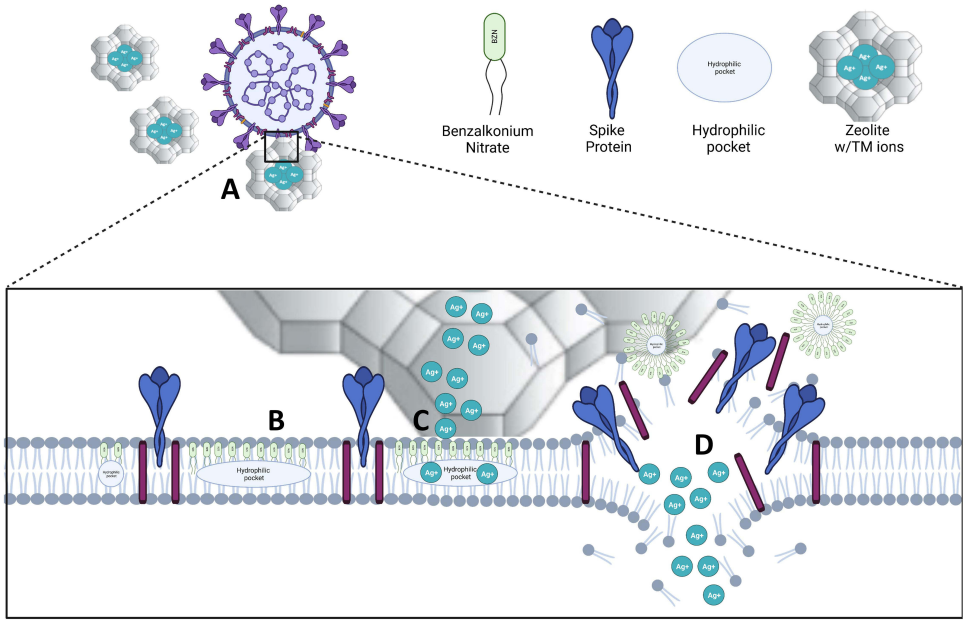

Figure 9 Diagram of antiviral mechanism of action against SARS-CoV-2. (**A**) TM-containing zeolites comes in contact with the viral particles via electrostatic charge. (**B**) Benzalkonium nitrate (BZN) permeates the envelope and forms hydrophilic pockets in the lipid bilayer. (**C**) Metal ions diffuse through the envelope and enter the virion, targeting the inner viral components. (**D**) BZN disrupts the viral envelope and induces greater metal ion influx.

quat to the bacteria leads to loss of intracellular components, which is not relevant for deactivating viruses since transport across the bilayer in envelope viruses is less important.[68]

The use of lower concentrations of both these active components to successfully inactivate viruses in real-world applications has both environmental and health implications. Several diseases such as asthma, chronic obstructive pulmonary disease are aggravated by quats.[62] At a biological level, the presence of quats in the blood have been correlated with increase in inflammatory markers, altered mitochondrial function and alteration of cholesterol homeostasis.[62] From an environmental perspective, the long persistence of quats in the environment, as well as possibility of quats discharging into water streams will have negative impacts on aquatic ecosystems as well as possibly contaminate food chains from water use in irrigation.[62,69,70] There is also concern about transition metals in the environment, because of the toxicity to microorganisms.[71] Fortunately for silver, the immobilization due to binding to soil humic acids, clays limit the available bioactive concentration.[72] Nevertheless, any technology that minimizes the amount of actives without sacrificing antiviral potency is of value.

Focusing on how to adapt the technology described in this paper in future practical applications is of relevance. We have only demonstrated the incorporation into textiles. Considering the extended stability of the aqueous nanozeolite suspensions along with water-soluble quat, it is conceivable that the materials can be readily incorporated into paints and coatings without issues of settling. The technology can also be used in aqueous sprays. The challenges with the technology are toxicity, especially inhalation toxicity if used as sprays, but should not be a problem with paints and coatings and incorporation into textiles.

Conclusions

This study introduces transition metal zeolite nanoparticles and in combination with quaternary ammonium compound as antiviral agents, and complements the large number of nanostructures that are finding applications in efforts to inhibit SARS-CoV-2 virus and control COVID-19 pandemic.[73,74] The use of silver and zinc ion nanozeolite (AM30) and silver and copper ion nanozeolite (AV30) formulations, alone and in combination with benzalkonium nitrate (BZN), as suspensions and coatings in cotton- and/or polyester-based fabrics as antiviral agents towards SARS-CoV-2 are significant for their use in real-world applications. More importantly, the studies with SARS-CoV-2 outlined in this paper suggests that similar activity of transition metal-zeolite in combination with BZN should be observed against other viruses, supporting the broad antiviral activity of this technology for the reduction of viral infections.

Abbreviations

BZN, benzalkonium nitrate; SARS-CoV-2, human severe acute respiratory syndrome coronavirus 2; COVID-19, coronavirus disease; AgNP, silver nanoparticles; mCT, minutes contact time; HCT, hours contact time.

Ethics Approval and Informed Consent

This research was approved and conducted according to Texas Biomedical Research Institute (Texas Biomed) Institutional Biosafety Committee (IBC) policies. Procedures involving live SARS-CoV-2 were done inside Texas Biomed BSL-3 facilities.

Consent for Publication

The authors consent to publish all the contents of this manuscript including images, videos, recordings.

Acknowledgments

The following reagent was deposited by the Centers for Disease Control and Prevention and obtained through BEI Resources, NIAID, NIH: SARS-Related Coronavirus 2, Isolate USA-WA1/2020, NR-52281. This work was supported by the Department of Defense through COVID Cares Act distributed to the US Air Force's 59th Medical Wing (MDW). The views expressed are those of the authors and do not reflect the official views or policy of the Department of Defense or its Components.

Author Contributions

All authors made a significant contribution to the work reported, whether that is in the conception, study design, execution, acquisition of data, analysis and interpretation, or in all these areas; took part in drafting, revising or critically reviewing the article; gave final approval of the version to be published; have agreed on the journal to which the article has been submitted; and agree to be accountable for all aspects of the work.

Disclosure

ZeoVation is a startup company that grew out of the research at The Ohio State University (OSU), and the authors from OSU are involved with the company. Prabir K. Dutta and Sweta Shrestha are financially supported by ZeoVation, Inc. Prabir K. Dutta, W. James Waldman and D. Knight have financial investments in ZeoVation. The authors report no other conflicts of interest in this work.

References

1. V'Kovski P, Kratzel A, Steiner S, Stalder H, Thiel V. Coronavirus biology and replication: implications for SARS-CoV-2. *Nat Rev Microbiol*. 2021;19(3):155–170. doi:10.1038/s41579-020-00468-6
2. Kampf G, Brüggemann Y, Kaba HEJ, et al. Potential sources, modes of transmission and effectiveness of prevention measures against SARS-CoV-2. *J Hosp Infect*. 2020;106:678–697. doi:10.1016/j.jhin.2020.09.022
3. Meyerowitz EA, Richterman A, Gandhi RT, Sax PE. Transmission of SARS-CoV-2: a review of viral, host, and environmental factors. *Ann Intern Med*. 2021;174:69–79. doi:10.7326/M20-5008
4. Kraay AN, Hayashi MAL, Berendes DM, et al. Risk for fomite-mediated transmission of SARS-CoV-2 in child daycares, schools, nursing homes, and offices. *Emerg Infect Dis*. 2021;27:1229. doi:10.3201/eid2704.203631
5. Mohamadi M, Babington-Ashaye A, Lefort A, Flahault A. Risks of infection with SARS-CoV-2 due to contaminated surfaces: a scoping review. *Int J Environ Res Public Health*. 2021;18:11019. doi:10.3390/ijerph182111019
6. EPA. Guidance for products adding residual efficacy claims; 2022. Available from: https://www.epa.gov/pesticide-registration/guidance-products-adding-residual-efficacy-claims. Accessed April 21, 2023.
7. Tiwari S, Juneja S, Ghosal A, et al. Antibacterial and antiviral high-performance nanosystems to mitigate new SARS-CoV-2 variants of concern. *Curr Opin Biomed Eng*. 2022;21:100363. doi:10.1016/j.cobme.2021.100363
8. Yasamineh S, Kalajahi HG, Yasamineh P, et al. An overview on nanoparticle-based strategies to fight viral infections with a focus on COVID-19. *J Nanobiotechnology*. 2022;20(1):440. doi:10.1186/s12951-022-01625-0
9. Dutta PK, Shrestha S, Wang B Silver in health and medicinal applications, e-book; 2021.
10. Jeremiah SS, Miyakawa K, Morita T, Yamaoka Y, Ryo A. Potent antiviral effect of silver nanoparticles on SARS-CoV-2. *Biochem Biophys Res Commun*. 2020;533:195–200. doi:10.1016/j.bbrc.2020.09.018
11. Merkl P, Long S, McInerney GM, Sotiriou GA. Antiviral activity of silver, copper oxide and zinc oxide nanoparticle coatings against SARS-CoV-2. *Nanomaterials*. 2021;11:1312. doi:10.3390/nano11051312
12. Dadashpour M, Firouzi-Amandi A, Pourhassan-Moghaddam M, et al. Biomimetic synthesis of silver nanoparticles using Matricaria chamomilla extract and their potential anticancer activity against human lung cancer cells. *Mater Sci Eng C Mater Biol Appl*. 2018;92:902–912. doi:10.1016/j.msec.2018.07.053
13. Chaudhary V, Mostafavi E, Kaushik A. De-coding Ag as an efficient antimicrobial nano-system for controlling cellular/biological functions. *Matter Us*. 2022;5(7):1995–1998. doi:10.1016/j.matt.2022.06.024
14. Zhang Q, Hu Y, Masterson CM, et al. When function is biological: discerning how silver nanoparticle structure dictates antimicrobial activity. *iScience*. 2022;25(7):104475. doi:10.1016/j.isci.2022.104475
15. Sabbani S, Gallego-Perez D, Nagy A, et al. Synthesis of silver-zeolite films on micropatterned porous alumina and its application as an antimicrobial substrate. *Micropor Mesopor Mat*. 2010;135:131–136. doi:10.1016/j.micromeso.2010.06.020
16. Nagy A, Harrison A, Sabbani S, et al. Silver nanoparticles embedded in zeolite membranes: release of silver ions and mechanism of antibacterial action. *Int J Nanomedicine*. 2011;6:1833–1852. doi:10.2147/IJN.S24019
17. Lee SH, Jun BH. Silver nanoparticles: synthesis and application for nanomedicine. *Int J Mol Sci*. 2019;20:865. doi:10.3390/ijms20040865
18. Crabtree JH, Burchette RJ, Siddiqi RA, Huen IT, Hadnott LL, Fishman A. The Efficacy of Silver-ion implanted catheters in reducing peritoneal dialysis-related infections. *Perit Dial Int*. 2003;23:368–374. doi:10.1177/089686080302300410
19. Roe D, Karandikar B, Bonn-Savage N, Gibbins B, Roullet JB. Antimicrobial surface functionalization of plastic catheters by silver nanoparticles. *J Antimicrob Chemother*. 2008;61:869–876. doi:10.1093/jac/dkn034
20. Hebeish A, El-Rafie MH, El-Sheikh MA, Seleem AA, El-Naggar ME. Antimicrobial wound dressing and anti-inflammatory efficacy of silver nanoparticles. *Int J Biol Macromol*. 2014;65:509–515. doi:10.1016/j.ijbiomac.2014.01.071
21. Elechiguerra JL, Burt JL, Morones JR, et al. Interaction of silver nanoparticles with HIV-1. *J Nanobiotechnology*. 2005;3:6. doi:10.1186/1477-3155-3-6
22. Galdiero S, Falanga A, Vitiello M, et al. Silver nanoparticles as potential antiviral agents. *Molecules*. 2011;16:8894–8918. doi:10.3390/molecules16108894
23. Sagripanti JL, Routson LB, Lytle CD. Virus inactivation by copper or iron ions alone and in the presence of peroxide. *Appl Environ Microbiol*. 1993;59:4374–4376. doi:10.1128/aem.59.12.4374-4376.1993
24. Jordan FT, Nassar TJ. The influence of copper on the survival of infectious bronchitis vaccine virus in water. *Vet Rec*. 1971;89:609–610. doi:10.1136/vr.89.23.609

25. Totsuka A, Otaki K. The effects of amino acids and metals on the infectivity of poliovirus ribonucleic acid. *Jpn J Microbiol*. 1974;18:107–112. doi:10.1111/j.1348-0421.1974.tb00797.x
26. Kittler S, Greulich C, Diendorf J, Koller M, Epple M. Toxicity of silver nanoparticles increases during storage because of slow dissolution under release of silver ions. *Chem Mater*. 2010;22:4548–4554. doi:10.1021/cm100023p
27. Auerbach SM, Carrado KA, Dutta PK. *Handbook of Zeolite Science and Technology*. CRC Press; 2003.
28. Dutta P, Wang B. Zeolite-supported silver as antimicrobial agents. *Coord Chem Rev*. 2019;383:1–29. doi:10.1016/j.ccr.2018.12.014
29. Walji SD, Bruder MR, Aucoin MG. Virus matrix interference on assessment of virucidal activity of high-touch surfaces designed to prevent hospital-acquired infections. *Antimicrob Resist Infect Control*. 2021;10:133. doi:10.1186/s13756-021-01001-x
30. Hodek J, Zajícová V, Lovětinská-šlamborová I, et al. Protective hybrid coating containing silver, copper and zinc cations effective against human immunodeficiency virus and other enveloped viruses. *BMC Microbiol*. 2016;16(Suppl 1):56. doi:10.1186/s12866-016-0675-x
31. Baker N, Williams AJ, Tropsha A, Ekins S. Repurposing quaternary ammonium compounds as potential treatments for COVID-19. *Pharm Res Dordr*. 2020;37:104. doi:10.1007/s11095-020-02842-8
32. Ogilvie BH, Solis-Leal A, Lopez JB, et al. Alcohol-free hand sanitizer and other quaternary ammonium disinfectants quickly and effectively inactivate SARS-CoV-2. *J Hosp Infect*. 2021;108:142–145. doi:10.1016/j.jhin.2020.11.023
33. Gerba CP. Quaternary ammonium biocides: efficacy in application. *Appl Environ Microbiol*. 2015;81:464–469. doi:10.1128/AEM.02633-14
34. Wang B, Li YZ, Shao CR, Cui MY, Dutta PK. Rapid and high yield synthesis method of colloidal nano faujasite. *Micropor Mesopor Mat*. 2016;230:89–99. doi:10.1016/j.micromeso.2016.05.001
35. Souza TGF, Ciminelli VST, Mohallem NDS. A comparison of TEM and DLS methods to characterize size distribution of ceramic nanoparticles. *J Phys Conf Ser*. 2016;733:012039. doi:10.1088/1742-6596/733/1/012039
36. EPA. Standard operating procedure for OECD quantitative method for evaluating bactericidal and mycobactericidal activity of microbicides used on hard, non-porous surfaces, MB-25-05. Available from: https://www.epa.gov/sites/default/files/2019-05/documents/mb-25-05.pdf. Accessed October 2, 2022.
37. Chen YN, Hsueh YH, Hsieh CT, Tzou DY, Chang PL. Antiviral activity of graphene-silver nanocomposites against non-enveloped and enveloped viruses. *Int J Environ Res Public Health*. 2016;13:430. doi:10.3390/ijerph13040430
38. Hosseini M, Chin AWH, Behzadinasab S, Poon LLM, Ducker WA. Cupric oxide coating that rapidly reduces infection by SARS-CoV-2 via solids. *ACS Appl Mater Interfaces*. 2021;13:5919–5928. doi:10.1021/acsami.0c19465
39. Balagna C, Perero S, Percivalle E, Nepita EV, Ferraris M. Virucidal effect against coronavirus SARS-CoV-2 of a silver nanocluster/silica composite sputtered coating. *Open Ceram*. 2020;1:100006. doi:10.1016/j.oceram.2020.100006
40. Butot S, Baert L, Zuber S. Assessment of antiviral coatings for high-touch surfaces by using human coronaviruses HCoV-229E and SARS-CoV-2. *Appl Environ Microbiol*. 2021;87:e0109821. doi:10.1128/AEM.01098-21
41. Flincec Grgac S, Tarbuk A, Dekanic T, Sujka W, Draczynski Z. The chitosan implementation into cotton and polyester/cotton blend fabrics. *Materials*. 2020;13:1616. doi:10.3390/ma13071616
42. Engelbrecht K, Ambrose D, Sifuentes L, et al. Decreased activity of commercially available disinfectants containing quaternary ammonium compounds when exposed to cotton towels. *Am J Infect Control*. 2013;41:908–911. doi:10.1016/j.ajic.2013.01.017
43. Hinchliffe DJ, Condon BD, Madison CA, Reynolds M, Hron RJ. An optimized co-formulation minimized quaternary ammonium compounds adsorption onto raw cotton disposable disinfecting wipes and maintained efficacy against methicillin-resistant Staphylococcus aureus, vancomycin-resistant Enterococcus faecalis, and Pseudomonas aeruginosa. *Text Res J*. 2018;88:2329–2338. doi:10.1177/0040517517720505
44. Kroll A, Pillukat MH, Hahn D, Schnekenburger J. Interference of engineered nanoparticles with in vitro toxicity assays. *Arch Toxicol*. 2012;86:1123–1136. doi:10.1007/s00204-012-0837-z
45. Imani SM, Ladouceur L, Marshall T, et al. Antimicrobial nanomaterials and coatings: current mechanisms and future perspectives to control the spread of viruses including SARS-CoV-2. *ACS Nano*. 2020;14:12341–12369. doi:10.1021/acsnano.0c05937
46. Goharshadi EK, Goharshadi K, Moghayedi M. The use of nanotechnology in the fight against viruses: a critical review. *Coord Chem Rev*. 2022;464:214559.
47. Minoshima M, Lu Y, Kimura T, et al. Comparison of the antiviral effect of solid-state copper and silver compounds. *J Hazard Mater*. 2016;312:1–7. doi:10.1016/j.jhazmat.2016.03.023
48. Roy S, Sarkhel S, Bisht D, Hanumantharao SN, Rao S, Jaiswal A. Antimicrobial mechanisms of biomaterials: from macro to nano. *Biomater Sci*. 2022;10:4392. doi:10.1039/D2BM00472K
49. Pal A, Goswami R, Roy DN. A critical assessment on biochemical and molecular mechanisms of toxicity developed by emerging nanomaterials on important microbes. *Environ Nanotechnol Monit Manag*. 2021;16:100485. doi:10.1016/j.enmm.2021.100485
50. Gavanji S, Larki B, Mehrasa M. A review of effects of molecular mechanism of silver nanoparticles on some microorganism and eukaryotic cells. *Tech J Eng Appl Sci*. 2013;3(1):48–58.
51. Rai M, Deshmukh SD, Ingle AP, Gupta IR, Galdiero M, Galdiero S. Metal nanoparticles: the protective nanoshield against virus infection. *Crit Rev Microbiol*. 2016;42:46–56. doi:10.3109/1040841X.2013.879849
52. Lara HH, Ayala-Nunez NV, Ixtepan-Turrent L, Rodriguez-Padilla C. Mode of antiviral action of silver nanoparticles against HIV-1. *J Nanobiotechnology*. 2010;8:1. doi:10.1186/1477-3155-8-1
53. Warnes Sarah L, Summersgill Emma N, Keevil CW. Inactivation of murine norovirus on a range of copper alloy surfaces is accompanied by loss of capsid integrity. *Appl Environ Microbiol*. 2015;81:1085–1091. doi:10.1128/AEM.03280-14
54. Vincent M, Duval RE, Hartemann P, Engels-Deutsch M. Contact killing and antimicrobial properties of copper. *J Appl Microbiol*. 2018;124:1032–1046. doi:10.1111/jam.13681
55. Korant B, Kauer J, Butterworth B. Zinc ions inhibit replication of rhinoviruses. *Nature*. 1974;248:588–590. doi:10.1038/248588a0
56. Liao L, Xiao W, Zhao M, et al. Can N95 respirators be reused after disinfection? How many times? *ACS Nano*. 2020;14:6348–6356. doi:10.1021/acsnano.0c03597
57. Ke Z, Oton J, Qu K, et al. Structures and distributions of SARS-CoV-2 spike proteins on intact virions. *Nature*. 2020;588:498–502. doi:10.1038/s41586-020-2665-2
58. Schrank CL, Minbiole KPC, Wuest WM. Are quaternary ammonium compounds, the workhorse disinfectants, effective against severe acute respiratory syndrome-coronavirus-2? *ACS Infect Dis*. 2020;6:1553–1557. doi:10.1021/acsinfecdis.0c00265

59. Obłąk E, Futoma-Kołoch B, Wieczyńska A. Biological activity of quaternary ammonium salts and resistance of microorganisms to these compounds. *World J Microbiol Biotechnol*. 2021;37. doi:10.1007/s11274-020-02978-0
60. Simon M, Veit M, Osterrieder K, Gradzielski M. Surfactants–compounds for inactivation of SARS-CoV-2 and other enveloped viruses. *Curr Opin Colloid Interface Sci*. 2021;55:101479. doi:10.1016/j.cocis.2021.101479
61. Wessels S, Ingmer H. Modes of action of three disinfectant active substances: a review. *Regul Toxicol Pharmacol*. 2013;67:456–467. doi:10.1016/j.yrtph.2013.09.006
62. Dewey HM, Jones JM, Keating MR, Budhathoki-Uprety J. Increased use of disinfectants during the COVID-19 pandemic and its potential impacts on health and safety. *ACS Chem Health Saf*. 2021;29:27–38. doi:10.1021/acs.chas.1c00026
63. Khokhar M, Roy D, Purohit P, Goyal M, Setia P. Viricidal treatments for prevention of coronavirus infection. *Pathog Glob Health*. 2020;114:349–359. doi:10.1080/20477724.2020.1807177
64. Bright KR, Sicairos-Ruelas EE, Gundy PM, Gerba CP. Assessment of the antiviral properties of zeolites containing metal ions. *Food Environ Virol*. 2009;1:37–41. doi:10.1007/s12560-008-9006-1
65. Tuladhar E, de Koning MC, Fundeanu I, Beumer R, Duizer E. Different virucidal activities of hyperbranched quaternary ammonium coatings on poliovirus and influenza virus. *Appl Environ Microbiol*. 2012;78:2456–2458. doi:10.1128/AEM.07738-11
66. Geller C, Varbanov M, Duval RE. Human coronaviruses: insights into environmental resistance and its influence on the development of new antiseptic strategies. *Viruses*. 2012;4:3044–3068. doi:10.3390/v4113044
67. Gilbert P, Moore LE. Cationic antiseptics: diversity of action under a common epithet. *J Appl Microbiol*. 2005;99:703–715. doi:10.1111/j.1365-2672.2005.02664.x
68. Springthorpe VS, Grenier JL, Lloyd-Evans N, Sattar SA. Chemical disinfection of human rotaviruses: efficacy of commercially-available products in suspension tests. *Epidemiol Infect*. 1986;97:139–161.
69. Hora PI, Arnold WA. Photochemical fate of quaternary ammonium compounds in river water. *Environ Sci*. 2020;22:1368–1381. doi:10.1039/d0em00086h
70. Hora PI, Pati SG, McNamara PJ, Arnold WA. Increased use of quaternary ammonium compounds during the SARS-CoV-2 pandemic and beyond: consideration of environmental implications. *Environ Sci Technol Lett*. 2020;7:622–631. doi:10.1021/acs.estlett.0c00437
71. Wijnhoven SW, Peijnenburg WJGM, Herberts CA, et al. Nano-silver–a review of available data and knowledge gaps in human and environmental risk assessment. *Nanotoxicology*. 2009;3:109–138. doi:10.1080/17435390902725914
72. Nowack B, Krug HF, Height M. 120 years of nanosilver history: implications for policy makers. *Environ Sci Technol*. 2011;45:1177–1183. doi:10.1021/es103316q
73. Sadique MA, Yadav S, Ranjan P, et al. High-performance antiviral nano-systems as a shield to inhibit viral infections: SARS-CoV-2 as a model case study. *J Mater Chem B*. 2021;9(23):4620–4642. doi:10.1039/d1tb00472g
74. Hashemi B, Akram FA, Amirazad H, et al. Emerging importance of nanotechnology-based approaches to control the COVID-19 pandemic; focus on nanomedicine iterance in diagnosis and treatment of COVID-19 patients. *J Drug Deliv Sci Technol*. 2022;67:102967. doi:10.1016/j.jddst.2021.102967

International Journal of Nanomedicine Dovepress

Publish your work in this journal

The International Journal of Nanomedicine is an international, peer-reviewed journal focusing on the application of nanotechnology in diagnostics, therapeutics, and drug delivery systems throughout the biomedical field. This journal is indexed on PubMed Central, MedLine, CAS, SciSearch®, Current Contents®/Clinical Medicine, Journal Citation Reports/Science Edition, EMBase, Scopus and the Elsevier Bibliographic databases. The manuscript management system is completely online and includes a very quick and fair peer-review system, which is all easy to use. Visit http://www.dovepress.com/testimonials.php to read real quotes from published authors.

Submit your manuscript here: https://www.dovepress.com/international-journal-of-nanomedicine-journal